Vol. 8, No. 4, August 2024, pp. 345-354

Current Optics and Photonics

Regular Paper

A Novel Frequency-octupling Millimeter Wave ROF Without Bit Walk-off Effect Based on MZM and an Insertion Pilot Signal

Bin Li, Xu Chen, Siyuan Dai, and Xinqiao Chen*

School of Information and Communication Engineering, Communication University of China, Beijing 100024, China

(Received January 29, 2024 : revised May 31, 2024 : accepted June 3, 2024)

The bit walk-off effect caused by fiber dispersion and carrier reuse in the base station (BS) are two key problems in radio-over-fiber (ROF) systems. In this paper, a novel frequency-octupling ROF system based on the Mach-Zehnder modulator (MZM) is proposed, which can overcome the bit walk-off effect and realize carrier reuse by inserting pilot signals. Theoretical analysis and simulation verification of the system are carried out. Under the condition of a Q factor greater than 6, the optical fiber transmission distance of the upper and lower links is more than 290 km and 80 km, respectively. The influence of the main device parameters of the system on the Q factor is analyzed when they deviate from their designed values. The system designed in this paper can not only effectively overcome the bit walk-off effect, but also solve the problem of downlink performance degradation and the limitation of tunability caused by conventional carrier reuse in ROF. The system can greatly increase the transmission distance and improve the performance of the system and has an important application prospect in ROF.

Keywords : Bit walk-off effect, Mach-Zehnder modulator (MZM), Millimeter wave (MMW), Pilot frequency, Radio-over-fiber (ROF)

OCIS codes : (060.2330) Fiber optics communications; (060.4510) Optical communications; (060.5060) Phase modulation

I. INTRODUCTION

Radio-over-fiber (ROF) is considered a promising technology for providing broadband wireless access services due to its advantages of high capacity and high flexibility [1–3]. In ROF systems, it is desired to generate frequencies higher than 60 GHz millimeter waves (MMW) directly in the optical domain [4] in order to simplify implementation and reduce cost. However, since the conventional electric domain method of generating MMW signals is limited by the electronic bottleneck of electronic devices, it is difficult to generate MMW signals with frequencies above 40 GHz, and the transmission distance and capacity of the signals are severely limited by the dispersion of optical fibers. Therefore, optical MMW technology, which generates MMW in the optical domain, has attracted the attention of a wide range of researchers for its characteristics such as the high frequency of the generated signals, stable signals, and high tunability.

The methods for generating MMW in the optical domain can be broadly categorized as follows: (1) direct modulation [5], (2) optical heterodyne [6, 7], (3) frequency upconversion [8], (4) external modulation [9], (5) nonlinear methods [*e.g.* four-wave mixing (FWM), stimulated Brillouin scattering (SBS), cross-phase modulation (XPM), and cross-gain modulation (XGM)] [10–12], and (6) optoelectronic oscillator (OEO) [13, 14]. Among these methods, external modulation methods have significant advantages such as high modulation bandwidth, high tunability, high frequency responsiveness, high spectral purity of the generated signal,

*Corresponding author: chenxinqiao9999@163.com, ORCID 0000-0001-8522-3227

Color versions of one or more of the figures in this paper are available online.

and excellent system stability. Therefore, the current research is focused on external modulation-based techniques [15].

The major commercially available external modulators include Mach-Zehnder modulators (MZM), phase modulators (PM), and polarization modulators (PoIM). MMW generation with PoIM requires careful control of device polarization and increases the cost of the system. MMW generation using PMs is less pure. Generation of MMWs using MZMs offers greater reliability, higher frequency multiplication factor (FMF), low phase noise, and frequency tunability; Therefore, it has become the main method for generating MMWs in the optical domain [16–20].

Conventional data modulation methods include double-sideband (DSB) modulation, single-sideband (SSB) modulation, and modulation with optical carrier suppression (OCS). DSB modulation has radio frequency (RF) signal periodic fading and the bit walk-off effect. OCS DSB has the bit walk-off problem. The conventional SSB's FMF is only 1. In the generation of an optical MMW based on an external modulator, the MMW is generated by beating the $\pm n^{th}$-order sidebands on PD. It can be considered as a generalized OCS DSB. It still has the bit walk-off effect problem. To solve the bit walk-off effect, one method is that the $-n^{th}$ (or $+n^{th}$)-order sideband is filtered out by a filter and the data is modulated on it first, then $\pm n^{th}$-order sidebands are combined and sent to a base station (BS). The problem with this method is that the application of optical filters increases the cost and power loss of the system, reduces the tunability of the system, etc. Therefore, it is important to generate OCS MMW signals without optical filters to overcome the bit walk-off effect of ROF systems. Arya and Zacharias [21] proposed a method to reduce the bit-walk off effect using an acousto-optic tunable filter and uniform fiber Bragg grating (FBG). This method needs a filter, adds cost, and reduces the tenability of the system. Guo *et al*. [22] proposed a method to reduce the bit-walk off effect by optimizing the transmission point of MZM. This method needs complex devices to control the MZM's transmission points.

To reduce the cost of the BS in ROF systems, carrier reuse is needed in the BS. The most common method for carrier reuse [23–25] is to reflect a portion of the n^{th} (or $-n^{th}$)-order idle sideband without data by a fiber Bragg grating (FBG) and the uplink data is modulated on it. This approach leads to two problems: One is that the operating frequency point of the FBG must be located in the n^{th}(or $-n^{th}$)-order optical sideband, which will lead to poor tunability of the system; The other is that since the FBG reflects part of the power of the n^{th}-order sideband, this will inevitably lead to an imbalance of the power in the $\pm n^{th}$-order sidebands, which will degrade the performance of the downlink.

To solve the above problems, a frequency-octupling MMW ROF system based on two MZMs connected in parallel with an inserting pilot signal is proposed and verified by simulation in this paper. At the central station (CS), an optical coupler is used to split the optical carrier from a laser diode (LD) into two beams sent to the upper branch and lower branch. The upper branch is used to generate $\pm 4^{th}$-order sidebands with the data modulated only on the $+4^{th}$-order sideband by adjusting the DC bias voltages of the two MZMs, the RF local oscillator (LO) voltages, phase index of the phase modulator, and the multiplication of the electrical gainer (EG). The lower branch is used as a pilot frequency signal. At the BS, the pilot frequency signal is reflected by the 100% reflectivity FBG and is used as a carrier for the uplink for carrier reuse. The signal output from the FBG is injected into the PD to generate a frequency-octupling MMW signal. Since the data are modulated on $+4^{th}$-order and 0^{th}-order optical sidebands, respectively, there is no periodic fading and bit walk-off effect caused by dispersion. This greatly extends the transmission distance and improves the performance of the ROF link.

II. SYSTEM DESIGN

Figure 1 shows the schematic structure of the frequency-octupling ROF system based on a dual parallel MZM. The system is built with two RF local oscillators (LO1, LO2), three electrical phase shifters (EPSs) (EPS1, EPS1, EPS3), a continuous-wave laser diode (LD), two 3 dB optical couplers (OC1, OC2), a dual-parallel MZM (DPMZM) (built with MZM1 and MZM2 in parallel), an FBG, an optical amplifier, an electrical amplifier, two photodetectors (PD1, PD2), an intensity modulator, an electrical phase modulator (PM), an EG, a mixer, a bandpass filter, two low-pass filters (LPF1, LPF2), and an optical switch. The dashed line in the figure indicates the circuit and the solid line indicates the optical path. The operating point of each MZM in the system is set at the maximum transmission point when the initial values of EPS1, EPS2, and EPS3 are set to 180°, 90°, and 180°, respectively. The structures of the DPMZM, the composite RF signal generator, and the data recovery circuits are labeled at the bottom of Fig. 1, respectively. The Composite RF signal module is used as the RF signal for the DPMZM. It is built with the EG, PM, and RF-LO1. The EG is used to amplify the data signal and the PM is used to modulate the data signal on the RF signal generated by the RF-LO1. The DPMZM module is used to generate $\pm 4^{th}$-order sidebands. It is built with the MZMi (i = 1, 2) and the EPSi (i = 1, 2, 3). The Recovery module is used to recover the downlink data signal in the BS. It is built with bandpass filter, mixer, LPF1, and RF-LO2.

At the CS, the optical carrier output from the LD is split into two signals by OC1, which are input to the upper and lower branches, which are composed of the DPMZM. The output signals of the upper and lower branches are synthesized into one signal by OC2, which is transmitted to the BS via optical fiber. The uplink signal from the BS to the CS is first injected into the PD2 for photoelectric conversion and then input into LPF2 to recover the uplink data signal.

In the BS, the pilot signal in the downlink signal is first

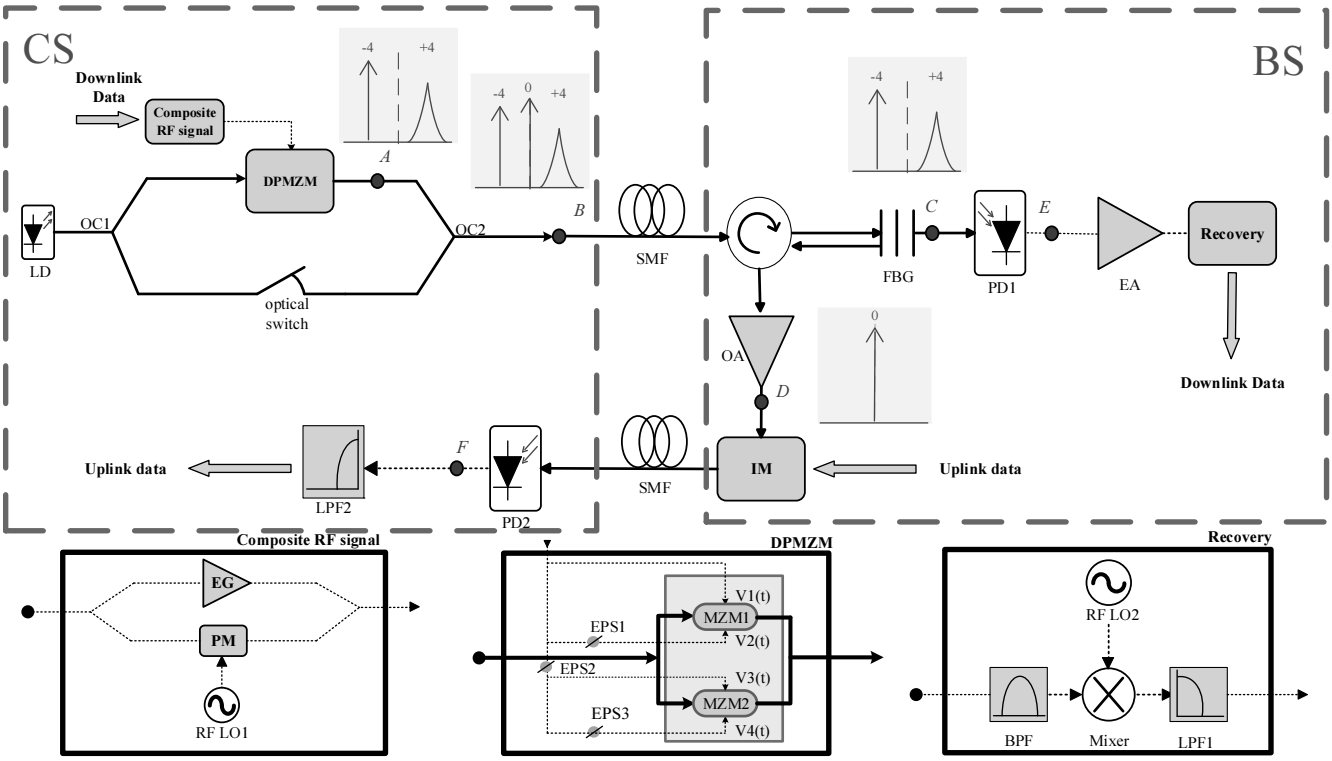

FIG. 1. Schematic diagram of the frequency-octupling ROF system based on MZM and insert pilot signal. BPF, bandpass filter; CS, central station; DPMZM, dual-parallel MZM; EA, electrical amplifier; EG, electrical gainer; EPS, electrical phase shifter; FBG, fiber Bragg grating; IM, intensity modulator; LD, laser diode; LO, local oscillator; LPF, low-pass filters; MZM, Mach-Zehnder modulators; OC, optical coupler; PD, photodetectors; PM, phase modulators; RF, radio frequency; ROF, radio-over-fiber; SMF, single-mode fiber.

reflected by the FBG, amplified by the optical amplifier, and then used as the optical carrier for the uplink, by which the uplink data signal is modulated on it through the IM, and transmitted back to the CS through the optical fiber. The optical signal filtered out of the pilot frequency signal is injected into the PD1 for optoelectronic conversion, and the frequency-octupling MMW signal with the downlink data signal is generated and the data signal is recovered from the downlink signal through the data recovery circuit.

III. OPERATION PRINCIPLE

3.1. The Output of the Central Station

The optical carrier from the LD is expressed as $E_0(t) = 4E_0 \exp(j\omega_0 t)$, where $4E_0$ and ω_0 are its amplitude and angular frequency of the optical carrier, respectively. We suppose that the binary data signal is expressed as $s(t) = \sum_n I_n g(t - nT)$, where $I_n \in \{0, 1\}$ is the binary sequence, $g(t)$ is the code form function, and T is the code duration.

The RF drive signal generated by LO1 is expressed as $V_{LO1}(t) = V_{RF}\cos(\omega_{RF} t)$, where V_{RF} and ω_{RF} are the amplitude and angular frequency of the RF drive signal, respectively. We set the magnification G of the EG to 6, the phase modulation index of the PM to $3\pi/8$, and the half-wave voltage V_π of the MZM to 4 V. Then the composite RF drive signals loaded onto the upper and lower arms of the two MZMs are expressed as follows:

$$V_i(t) = V_{RF}\cos\left[\omega_{RF} t + \frac{3\pi}{8}s(t) + \varphi_i\right] + 6s(t), \tag{1}$$

where $\varphi_i = 0, \pi, \pi/2, 3\pi/2 (i = 1, 2, 3, 4)$, $\varphi_i = (i = 2, 3, 4)$ is generated by EPS1, EPS2 and EPS3, respectively.

The output of MZM1 is expressed as follows:

$$\begin{aligned} E_{MZM1} &= E_0 \exp\left[j\left\{\omega_0 t + \pi\frac{V_{RF}}{V_\pi}\cos\left[\omega_{RF} t + \frac{3\pi}{8}s(t)\right] + \pi\frac{G}{V_\pi}s(t)\right\}\right] + \\ &E_0 \exp\left[j\left\{\omega_0 t + \pi\frac{V_{RF}}{V_\pi}\cos\left[\omega_{RF} t + \frac{3\pi}{8}s(t) + \pi\right] + \pi\frac{G}{V_\pi}s(t)\right\}\right] \\ &= 2E_0 \exp(j\omega_0 t)\sum_{n=-\infty}^{\infty}(-1)^n J_{2n}(m)\exp\left\{j2n\left[\omega_{RF} t + \frac{3\pi}{8}s(t)\right] + j\frac{3\pi}{2}s(t)\right\}, \end{aligned} \tag{2}$$

where $m = \pi V_{RF}/V_\pi$ is the modulation index of MZM1. Here, the equation $\exp(jx\cos\theta) = \sum_{n=-\infty}^{\infty} j^n J_n(x)\exp(jn\theta)$ is used.

The structure of MZM2 is the same as that of MZM1, and the initial phase of the composite RF driving signal loaded into MZM2 differs from that of MZM1 by 90°, the output signal of the DPMZM is expressed as follows:

$$\begin{aligned}
&E_{\mathrm{DPMZM}}=E_{\mathrm{MZM1}}+E_{\mathrm{MZM2}}\\
&=E_0\exp(j\omega_0 t)\left\{\sum_{n=-\infty}^{\infty}2(-1)^n J_{2n}(m)\exp\left\{j2n\left[\omega_{\mathrm{RF}}t+\frac{3\pi}{8}s(t)\right]+j\frac{3\pi}{2}s(t)\right\}+\right.\\
&\left.\sum_{n=-\infty}^{\infty}2(-1)^n J_{2n}(m)\exp\left\{j2n\left[\omega_{\mathrm{RF}}t+\frac{3\pi}{8}s(t)\right]+j\frac{3\pi}{2}s(t)\right\}\right\}\\
&=E_0\exp(j\omega_0 t)\sum_{n=-\infty}^{\infty}\left[2\left[1+(-1)^n\right]J_{2n}(m)\exp\left\{j2n\left[\omega_{\mathrm{RF}}t+\frac{3\pi}{8}s(t)\right]+j\frac{3\pi}{2}s(t)\right\}\right]\\
&=E_0\exp(j\omega_0 t)\sum_{n=-\infty}^{\infty}\left[4J_{4n}(m)\exp\left\{j4n\left[\omega_{\mathrm{RF}}t+\frac{3\pi}{8}s(t)\right]+j\frac{3\pi}{2}s(t)\right\}\right],
\end{aligned}\tag{3}$$

when m is chosen as 2.4048, there are $J_0(2.4048) = 1.327 \times 10^{-5}$, $J_4(2.4048) = 0.0647$, $J_8(2.4048) = 9.216 \times 10^{-5}$…

Then $P_4/P_0 = 20\lg[J_4(2.4048) / J_0(2.4048)] = 73.76$ dB, $P_4/P_8 = 20\lg[J_4(2.4048) / J_8(2.4048)] = 56.93$ dB. We can see that all the sidebands except the ±4$^{\mathrm{th}}$-order sidebands are effectively suppressed. Omitting the sidebands except ±4$^{\mathrm{th}}$, Eq. (3) can be simplified as follows:

$$\begin{aligned}
E_{\mathrm{DPMZM}}(0,t)=E_0\{&J_4(m)\exp\left[j(\omega_0 t+4\omega_{\mathrm{RF}}t)+j\pi s(t)\right]+\\
&J_{-4}(m)\exp\left[j(\omega_0 t-4\omega_{\mathrm{RF}}t)\right]\}.
\end{aligned}\tag{4}$$

From Eq. (4), we can see that the data is modulated only on the +4$^{\mathrm{th}}$ sideband. The output signals of the CS are the combined signals of the upper and lower branch signals via OC2, and can be expressed as follows:

$$\begin{aligned}
&E_{\mathrm{out}}=E_{\mathrm{DPMZM}}+E_c\\
&=E_0\left\{J_4(m)\exp\left[j(\omega_0 t+4\omega_{\mathrm{RF}}t)+j\pi s(t)\right]+J_{-4}(m)\exp\left[j(\omega_0 t-4\omega_{\mathrm{RF}}t)\right]\right\}+\\
&E_0\exp(j\omega_0 t).
\end{aligned}\tag{5}$$

3.2. Signal of the Base Station

3.2.1. Back-to-back System

In the case of back-to-back (BTB), at the BS, the expression of the signals transmitted from the CS to the BS is the same as Eq. (5). After filtering the pilot signals for carrier reuse, the output of the FBG is ±4$^{\mathrm{th}}$-order sidebands, the expression of which is the same as Eq. (4). The signal is injected into the PD1 for frequency beating, and the output signal of the PD1 is expressed as follows:

$$I(0,t)=\mu\left|E_{\mathrm{out}}(0,t)\right|^2=2\mu E_0^2 J_4^2(m)\left\{1+\cos\left[8\omega_{\mathrm{RF}}t+\pi s(t)\right]\right\},\tag{6}$$

where μ is the responsivity of the PD1.

3.2.2. Fiber Optic Transmission System

In the case of the optical fiber transmission system, ±4$^{\mathrm{th}}$-order sideband signals have different group velocities due to the effect of the chromatic dispersion of the fiber, and the output signal is expressed as follows:

$$\begin{aligned}
&E_{\mathrm{out}}(z,t)=E_{\mathrm{DPMZM}}(z,t)+E_c(z,t)\\
&=\exp(-\gamma z)E_0 J_4(m)\exp\left\{j\left[\omega_0 t+4\omega_{\mathrm{RF}}t-\beta(\omega_0+4\omega_{\mathrm{RF}})z\right]+j\pi s(t-t')\right\}+\\
&\exp(-\gamma z)E_0 J_{-4}(m)\exp\left\{j\left[\omega_0 t-4\omega_{\mathrm{RF}}t-\beta(\omega_0-4\omega_{\mathrm{RF}})z\right]\right\}+\\
&\exp(-\gamma z)E_0\exp\left[j(\omega_0 t-\beta\omega_0 z)\right],
\end{aligned}\tag{7}$$

where z is the transmission distance of optical fiber, $t' = (\omega_0 + 4\omega_{\mathrm{RF}})^{-1}\beta(\omega_0 + 4\omega_{\mathrm{RF}})z$ is the time delay of the code word, γ is the fiber loss coefficient, and $\beta(\omega)$ is the fiber transmission constant. The effect of fiber nonlinearity is neglected here.

Comparing Eq. (7) with Eq. (5), it can be seen that the spectrum of the signal after fiber transmission has not changed. Expanding the $\beta(\omega_0 \pm 4\omega_{\mathrm{RF}})$ in Eq. (7) with Taylor expansion and ignoring the higher terms with very small amplitudes $\beta^{(n)}(\omega_0)(n > 2)$, we get

$$\beta(\omega_0\pm4\omega_{\mathrm{RF}})\approx\beta(\omega_0)\pm4\omega_{\mathrm{RF}}\beta'(\omega_0)+8\omega^2{}_{\mathrm{RF}}\beta''(\omega_0),\tag{8}$$

substitute Eq. (8) into Eq. (7). After filtering out the pilot signal, the output of FBG is ±4$^{\mathrm{th}}$-order sidebands. After beating the ±4$^{\mathrm{th}}$-order sidebands in the PD1, the output signal of PD1 is expressed as follows:

$$\begin{aligned}
&I(z,t)=\mu\left|E_{\mathrm{out}}(z,t)\right|^2\\
&=2\exp(-2\gamma z)\mu E_0^2 J_4^2(m)\left\{1+\cos\left[\begin{array}{l}8\omega_{\mathrm{RF}}t+\beta(\omega_0+4\omega_{\mathrm{RF}})z-\\ \beta(\omega_0-4\omega_{\mathrm{RF}})z-\pi s(t-t')\end{array}\right]\right\}\\
&=2\exp(-2\gamma z)\mu E_0^2 J_4^2(m)\left\{1+\cos\left[8\omega_{\mathrm{RF}}t+8\omega_{\mathrm{RF}}\beta'(\omega_0)z-\pi s(t-t')\right]\right\}.
\end{aligned}\tag{9}$$

Here we substitute Eq. (8) into Eq. (7). From Eq. (9), it can be seen that there is no bit walk-off effect except for the influence of the fiber transmission delay.

IV. SIMULATION EXPERIMENT

4.1. Simulation Parameter Setting

According to Fig. 1, a simulation link is set up with Optisystem photon simulation software (OptiSystem Co., Nowy Sącz, Poland). The main values of the parameters in our simulation are shown in Table 1.

The values of the main parameters in Table 1 are determined as follows: The values of the continuous wave laser, data, frequency of RF-LO1 and V_π are given by the default values of the OptiSystem simulation software. The value of the amplitude of RF-LO1 is determined by the m of the MZM, which is chosen as 2.4048 in Section 3. The values of G and M are determined by Eq. (11) when the n is chosen as +4.

4.2. Simulation Experiment Results

Figure 2 shows spectrums at each point of Fig. 1: Figure 2(a) is the optical spectrum of point A, from which we can see that all the sidebands are suppressed except the ±4$^{\mathrm{th}}$-order sidebands; The peak power of the +4$^{\mathrm{th}}$-order sideband

is lower than that of the -4^{th}-order; There is no modulation of the data signal in the -4^{th}-order sideband, and the data is only modulated into the $+4^{th}$-order sideband. Figure 2(b) is the optical spectrum of point B with 0^{th}-order sideband labeled as the inserted pilot frequency signal.

Figure 2(c) is the optical spectrum of point C, which shows the $\pm4^{th}$-order sidebands of the downlink signal after filtering out the pilot signal. The spectrum shape is similar to that of Fig. 2(a). Figure 2(d) is the optical spectrum of point D, from which we can see that the uplink data has been modulated onto the pilot signal. Figure 2(e) is the spectrum of point E, it is the frequency-octupling MMW signal with the downlink data signal. Figure 2(f) is the spectrum of point F, which is the baseband signal carrying the uplink data signal.

TABLE 1. Main values of the parameters in the simulation system

Device	Parameter	Value
CW	Frequency (THz)	193.1
	Linewidth (MHz)	10
Data	Speed (Gbit/s)	2.5
RF-LO1	Frequency (GHz)	10
	Amplitude (V)	3.06188
Phase Modulator	M	$3\pi/8$
Electrical Gainer	G	6
MZM	V_π	4 V

In Fig. 3, the relation of the Q-factor with transmission fiber distance in the downlink of the proposed system is shown, and eye diagrams of the data signals out of the transmission fiber distances of 0 km (BTB), 20 km, 60 km, and 80 km are marked in the figure. From Fig. 3, the distance of the transmission fiber can be up to 80 km under the condition that the Q-factor is more than 6.

Figure 4 shows the relationship between the bit error ratio (BER) and the received power of PD1 and PD2 for 2.5 Gbit/s data in our designed system. As seen in Fig. 4(a), in the downlink, the power penalty is 0.4 dB and 0.85 dB for fiber optic transmission distances of 20 km and 40 km, respectively. As seen in Fig. 4(b), in the uplink, the power penalty is 0.19 dB and 0.33 dB for fiber optic transmission distances of 20 km and 40 km, respectively.

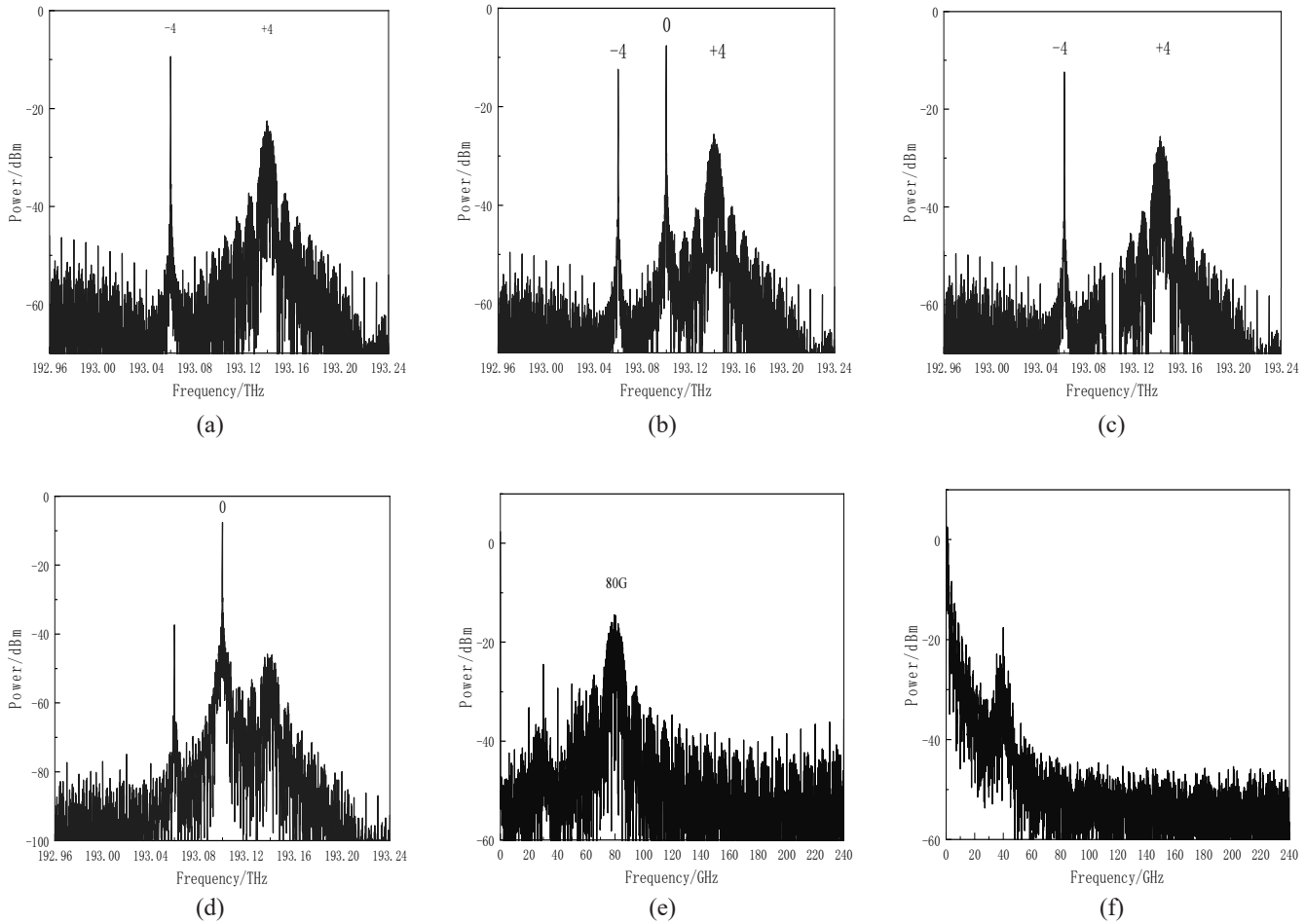

FIG. 2. Optical spectrum in Fig. 1 at (a) point A, (b) point B, (c) point C, (d) point D, (e) point E, and (f) point F.

V. SYSTEM STABILITY

The values of the parameters in our simulation link are the values from our theoretical analysis or the default values of simulation software. In practical applications, the values of the parameters often deviate from these theoretical values or default values due to changes in the environment and the limitations of device fabrication, and will inevitably affect the performance of the system. It is necessary to analyze this, and this issue is the stability of the system.

In the practical system, the main parameters that affect the Q factor the most are as follows: (1) the extinction ratio of the MZMs; (2) the RF driving voltage; (3) the phase modulation index of the PM; and (4) the magnification of the EG. The effect to suppress the spurious sidebands is increased with the extinction ratio of the MZM. The value of the RF voltage determines the modulation index of the MZMs, which directly affects the generation of desired sidebands. According to a previous analysis, the modulation index of PM and the magnification of the EG directly affect the single sideband modulation of the data.

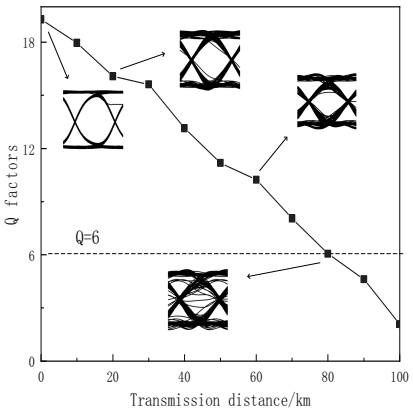

FIG. 3. Curve of Q factor as a function of fiber transmission distance.

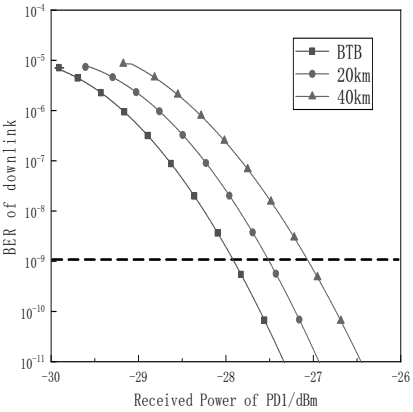

(a)

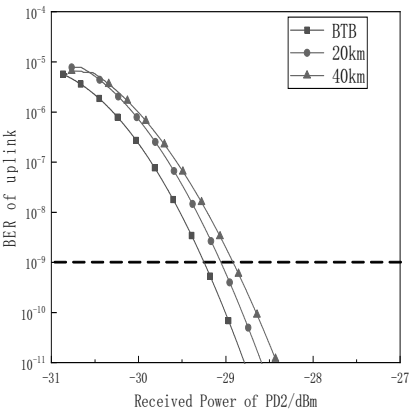

(b)

FIG. 4. The relationship between the bit error ratio (BER) and the received power of PD1 and PD2 in our designed system: (a) Downlink, (b) uplink.

5.1. Effect of Extinction Ratio of MZMs

Figure 5 shows the relationship between the extinction ratio of the MZM and the Q factor of the downlink. As seen in Fig. 5, in the case of BTB and 20 km of transmission fiber, when the extinction ratio reaches 30 dB, the Q factor of downlink data transmission remains basically unchanged as the extinction ratio grows. In the case of 40 km of transmission fiber, when the extinction ratio reaches 40 dB, the Q factor of downlink data transmission remains basically unchanged as the extinction ratio increases.

5.2. Effect of Modulation Index of MZMs

According to a previous analysis, the theoretical value of m is 2.4048. According to $m = \pi V_{RF}/V_{\pi}$, the default V_{π} = 4 V in the system, the V_{RF} value can be obtained as 3.06188 V. When the V_{RF} changes in the range of deviation from the theoretical within ±0.5 V, that is, 2.56188 V < V_{RF} < 3.56188 V, the corresponding m is in the range of 2.0121 < m < 2.7975. The relationship between the V_{RF} and the Q factor is shown in Fig. 6. From Fig. 6, it can be seen that when the V_{RF} is less than the theoretical value of 3.06188 V, the system performance is more sensitive to the deviation of the V_{RF}, and when the V_{RF} varies in the range of 2.876 V–3.407 V, Q > 6 is satisfied.

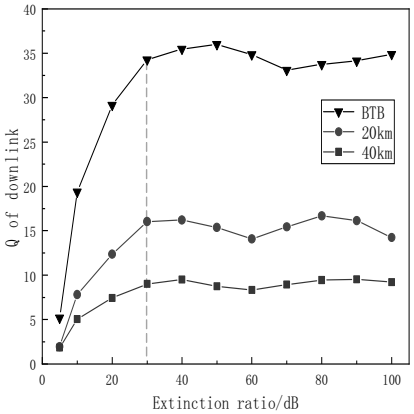

FIG. 5. Relation between Q factor with extinction ratio.

5.3. Effect of the Phase Modulation Index M of the Phase Modulator PM

According to a previous analysis, the theoretical value of the PM's phasing index M is 67.5°. When M varies in the range of 60°–75°, the relationship between M and Q factor is as shown in Fig. 7. As seen in Fig. 7, when M varies in the range of 61.2°–73.2°, $Q > 6$ is satisfied.

5.4. Effect of the Amplification G of the EG

According to a previous analysis, the design value of G is 6. When G varies in the range of 4.5 to 7.5, the relationship between G and the system Q factor is shown in Fig. 8. As seen in Fig. 8, the system performance is more sensitive to the deviation of the EG when G is less than the theoretical value of 6. As seen in Fig. 8, the Q factor decreases rapidly as G deviates from the theoretical value; When G varies in the range of 5.2 to 6.9, $Q > 6$ is satisfied.

5.5. Effect of EPS

The 90° EPS in the system is used to suppress the sidebands of the $2n$ (n is an odd number) optical sidebands from the two MZM output signals in the DPMZM. When it deviates from 90°, the undesired optical sidebands can't be completely suppressed, and it will degraded the performance of the system. In a parameter sweeping experiment for 90° EPS in the range of 90° ± 8°, the relationship between the deviation of phase of the EPS and the Q factor is obtained and shown in Fig. 9. It can be seen in Fig. 9 that for the value of 90° EPS in the range of 85.19°–92.38°, $Q > 6$ is satisfied.

5.6. Effects of M and G

The effects on the Q factor when the modulation index M of the PM and the amplification G of the EG deviate from the theoretical value are analyzed above. In practical applications, M and G often deviate from the theoretical values at the same time. Figure 10 shows the relationship between the Q factor with M and G. In Fig. 10, the black lines indicate a Q factor greater than 6, and the black points are the Q factor when $G = 6$, $M = 67.5°$. It can be seen that when the design values of $G = 6$, $M = 67.5°$ are used, the Q factor of the system reaches a peak value of 12.82, and the system performs optimally. The stability is summarized in Table 2.

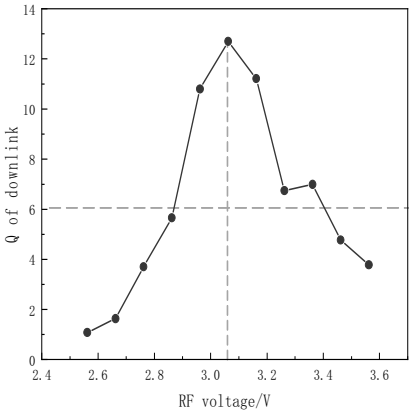

FIG. 6. Relation between Q factor and V_{RF}.

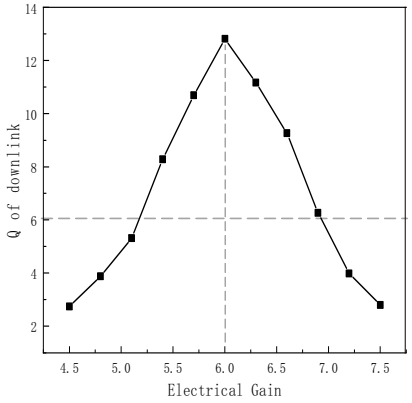

FIG. 8. Relation between G of EG and system Q factor.

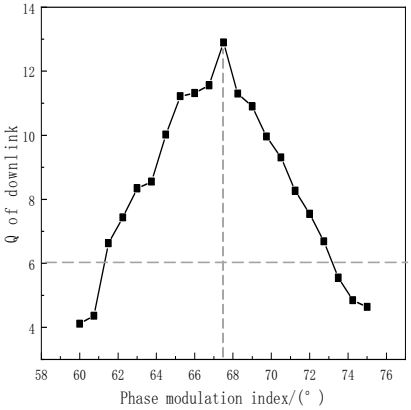

FIG. 7. Relation between Q factor and phase modulation index.

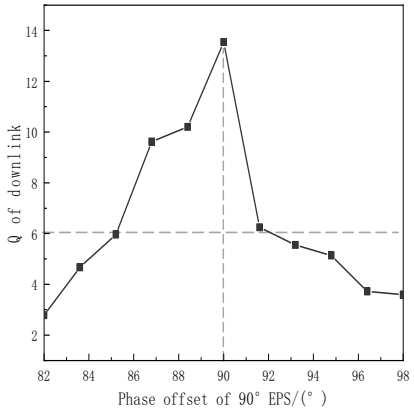

FIG. 9. Relation between the phase of the 90°EPS and Q factor.

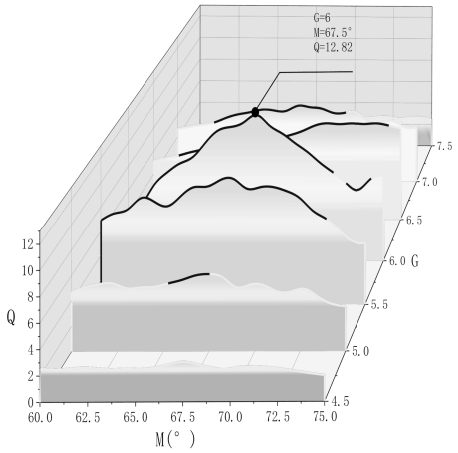

FIG. 10. Relation between Q factor with M and G.

TABLE 2. Summarizing stability

Device Parameters	Standard Value	Range of Deviation
Extinction of MZM (dB)	100	>40
m	2.4048	2.2588–2.6758
M	$3\pi/8$	61.2°–73.2°
G	6	5.2–6.9
90° EPS (°)	90	85.19–92.38

VI. DISCUSSION

6.1. Methods of Carrier Reuse

Carrier reuse is one of the important ways to reduce the cost of the BS. The most common method of carrier reuse in a frequency multiplication MMW ROF system is to reflect a portion of the idle sideband and use it as an optical carrier for the uplink. This method leads to degradation of downlink performance and system tunability.

To compare the advantages of our proposed scheme, an optical switch (OS) is added in Fig. 1. When the OS is closed, the system is the one discussed above. When the switch is opened, the data signal is modulated to the $+4^{th}$-order sideband. At the BS, the center reflection frequency of the FBG is set at the -4^{th}-order sideband, and the reflected -4^{th}-order sideband is used as an optical carrier for the uplink for carrier reuse.

In the conventional carrier reuse scheme, the center reflection frequency of the FBG must be located in the -4^{th}-order sideband as $f_0 - 4f_{RF}$, which varies with the change of f_{RF}. The tunability of the system is poor. Meanwhile, the reflectivity of the FBG directly affects the performance of the uplink and downlink; the larger the reflectivity is, the better the uplink performance is and the worse the downlink performance is, and vice versa. In our designed scheme of carrier reuse using the inserting pilot signal, the FBG center reflection frequency and reflectivity are both fixed as f_0 and 100%, respectively, and the system is very tunable.

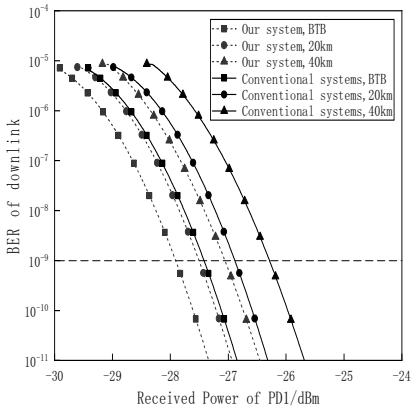

FIG. 11. Relation between bit error rate (BER) and received power of photodetector 1 (PD1).

Figure 11 shows the BER of downlink versus the received power of PD1 in the systems for the case of BTB, 20 km and 40 km transmission distances. As can be seen in Fig. 11, comparing the method using the inserted pilot frequency with the method of using a partially reflected -4^{th}-order sideband for carrier reuse, the sensitivity of PD1 improved by about 0.5 dB.

6.2. The Choice of G and M

According to the analysis above, the amplitudes of the $\pm n^{th}$ order sidebands for a binary data signal are proportional to $\exp\{j[n\omega_{RF}t + nMs(t)] + j\pi Gs(t)/V_\pi\}$ and $\exp\{-j[n\omega_{RF}t + nMs(t)] + j\pi Gs(t)/V_\pi\}$, respectively.

To modulate the data signal on the $+n^{th}$-order optical sideband only, the following equation needs to be satisfied.

$$\begin{cases} nM + \pi G/V_\pi = (2k_1 + 1)\pi \\ -nM + \pi G/V_\pi = 2k_2\pi \end{cases}, \tag{10}$$

where n is the order of the sidebands, and k_1 and k_2 are integers.

According to Eq. (10), we can get

$$G = (k + 1/2)V_\pi, M = (k' + 1/2)\pi/n, \tag{11}$$

where $k = k_1 + k_2$ and $k' = k_1 - k_2$ are integers.

According to Eq. (11), to modulate the data only on the $+4^{th}$-order sideband, when $k = k' = 1$, we get G and M as 6 and $3\pi/8$ ($V_\pi = 4$), respectively.

6.3. Nonlinear Effect in Optical Fiber

Since we designed the system with relatively low power, we did not consider the nonlinear effects of the fiber. In a wavelength division multiplexing (WDM) ROF system, the transmission power of the system is higher, and the nonlinear effect of the fiber needs to be considered.

6.4. Choosing the Reflectivity of the FBG

To compare the inserting pilot guide method proposed in this paper and the conventional method to realize carrier re-

use by using the reflected partially free -4^{th}-order sideband, we add an optical switch (OS) at the CS. But when the OS is closed, it is the inserting pilot system, at which time the FBG in the BS is used to reflect the pilot signal, and its reflected frequency is at the central carrier with a 100% transmission rate. However, when the OS is open, it is a carrier reuse system using the -4^{th}-order sideband, and the frequency of reflection of the FBG in the BS is located at the -4^{th}-order edge. According to the analysis of Chen *et al*. [25], the uplink and downlink performance are best when the reflectivity of the FBG is chosen as 5%.

VII. CONCLUSIONS

In this paper, a frequency-octupling MMW ROF system without a bit walk-off effect is proposed. At the center station, the optical carrier output from the LD is divided into two beams and input to the upper and lower branches. The upper branch consists of a DPMZM, and the lower branch is used as a pilot frequency signal. In the case of no data transmission, the output signal of the DPMZM is $\pm4^{th}$-order sidebands by adjusting the amplitude and initial phase of the RF drive signal loaded onto the DPMZM. In the case of data transmission, the RF driving signal is the composite RF signal, which is formed by combining two branch data signals. One data signal is formed by the data amplified by the EG and other data signal is formed by the data modulating the RF driving signal by a PM. By adjusting the phase modulation index M of the PM and the multiplication of the EG, the data signal is modulated only to the $+4^{th}$-order sideband. At the BS, carrier reuse is realized by reflecting the pilot frequency signal through the FBG for the optical carrier of the uplink. The $\pm4^{th}$-order sidebands through the FBG are beat in the PD to generate an MMW signal carrying the downlink data signal.

Since the uplink and downlink data signals are modulated to the pilot frequency signal and the $+4^{th}$-order sideband, respectively, the system overcomes the bit walk-off effect caused by fiber dispersion, and the length of the uplink and downlink transmission fibers can reach 290 km and 80 km, respectively, under the condition of guaranteeing that the Q factor is greater than 6. With 20 km, and 40 km transmission fiber lengths, the power penalty of the uplink is 0.19 dB and 0.33 dB, and the power penalty of the downlink is 0.4 dB and 0.85 dB, respectively.

The stability of the system is analyzed, the MZM extinction ratio is above 30 dB, the RF driving signal amplitude is in the range of 2.876 V–3.407 V, the M of PM is in the range of 61.2°–73.2°, the G of the EG is in the range of 5.2–6.9, the 90° EPS varies in the range of 85.19°–92.38°, and the Q factor is greater than 6, which can satisfy the transmission requirements of the system.

The main innovation of our proposed scheme designed is that the system not only effectively solves the bit walk-off effect problem and greatly improves the fiber transmission distance, but also solves the problems of downlink performance degradation and poor system tunability caused by conventional carrier reuse, which has important application prospects in MMW ROF systems.

FUNDING

Fundamental Research Funds for the Central Universities (Grant No. 3132018XNG1856, Grant No. 2018CUCTJ084).

ACKNOWLEDGMENTS

This work was supported by the Fundamental Research Funds for the Central Universities (Grant No. 3132018XNG1856, Grant No. 2018CUCTJ084).

DISCLOSURES

The authors declare that they have no known competing financial interests or personal relationships that could have appeared to influence the work reported in this paper.

DATA AVAILABILITY

All data generated or analyzed during this study are included in this published article.

REFERENCES

1. C. C. Cui and S. C. Chan, "Performance analysis on using period-one oscillation of optically injected semiconductor lasers for radio-over-fiber uplinks," IEEE J. Quantum. Electron. **48**, 490–499 (2012).
2. X. Qi, J. Liu, X. Zhang, and L. Xie, "Fiber dispersion and nonlinearity influences on transmissions of AM and FM data modulation signals in radio-over-fiber system," IEEE J. Quantum. Electron. **46**, 1170–1177 (2010).
3. W.-G. Hu, Y.-F. Shao, A.-R. Wang, C. Chen, L.-J. Yang, W.-C. Li, H.-N. Liu, Q.-Q. Jin, J.-G. Yue, and Y.-L. Zhang, "Research progress of externally modulated frequency-doubling optical millimeter wave," Laser J. (to be published).
4. H. Chi and J. Yao, "Frequency quadrupling and upconversion in a radio over fiber link," J. Light. Technol. **26**, 2706–2711 (2008).
5. L. Chen, Y. Pi, H. Wen, and S. Wen, "All-optical mm-wave generation by using direct modulation DFB laser and external modulator," Microw. Opt. Technol. Lett. **49**, 1265–1267 (2007).
6. C. Browning, A. Delmade, Y. Lin, D. H. Geuzebroek, and L. P. Barry, "Optical heterodyne millimeter-wave analog radio-over-fiber with photonic integrated tunable lasers," in Optical Fiber Communications Conference and Exhibition (OFC) (Optical Society of America, 2019), paper W1I.4.
7. X. Li, J. Xiao, Y. Xu, and J. Yu, "QPSK vector signal generation based on photonic heterodyne beating and optical carrier suppression," IEEE Photonics J. **7**, 7102606 (2015).

8. C. Wang, Q. Zhang, and W. Wang, "Low-frequency wideband vibration energy harvesting by using frequency up-conversion and quin-stable nonlinearity," J. Sound Vib. **399**, 169–181 (2017).
9. C. Zhang, T. G. Ning, J. Li, L. Pei, C. Li, S. Ma, "A full-duplex WDM-RoF system based on tunable optical frequency comb generator," Opt. Commun. **344**, 65–70 (2015).
10. M. Junker, T. Schneider, K.-U. Lauterbach, R. Henker, M. J. Ammann, and A. T. Schwarzbacher, "High quality millimeter wave generation via stimulated Brillouin scattering," in *Proc. 2007 Conference on Lasers and Electro-Optics (CLEO)* (Baltimore, MD, USA, May 6–11, 2007), pp. 1–2.
11. T. Wang, M. Chen, H. Chen, and S. Xie, "Millimetre-wave signal generation using FWM effect in SOA," Electron. Lett. **43**, 36–38 (2007).
12. H.-Y. Chen, Y.-C. Chi, C.-Y. Lin, C.-T. Tsai, and G.-R. Lin, "Four-wave-mixing suppression of master-to-slave injection-locked two-wavelength FPLD pair for MMW-PON," J. Light. Technol. **34**, 4810–4818 (2016).
13. G. Brunetti, M. N. Armenise, and C. Ciminelli, "Chip-scaled ka-band photonic linearly chirped microwave waveform generator," Front. Phys. **10**, 785650 (2022).
14. W. Li, F. Kong, and J. Yao, "Arbitrary microwave waveform generation based on a tunable optoelectronic oscillator," J. Light Technol. **31**, 3780–3786 (2013).
15. R. B. Chaudhuri, A. D. Barman, and A. Bogoni, "Photonic 60 GHz sub-bands generation with 24-tupled frequency multiplication using cascaded dual parallel polarization modulators," Opt. Fiber Technol. **58**, 102244 (2020).
16. A. B. Dar, F. Ahmad, and R. K. Jha, "Filterless optical millimeter-wave generation using cascaded-parallel Mach-Zehnder modulators with tunable frequency multiplication factor," Opt. Quant. Electron. **53**, 56 (2021).
17. Y. Pang, H. Ma, Y. Yan, and G. Liu, "A filterless scheme of generating frequency 16-tupling mm Wave based on triple-parallel MZM," Laser J. **45**, 45–49 (2024).
18. Z. Meng, F. Zhao, B. Y. Tian, B. Tian, X. Wang, X. Yang, and L. Zhao, "Analysis of vector millimeter wave signal transmission performance based on dual parallel MZM modulators," J. Optoelectron. **33**, 1183–1191 (2022).
19. Z. Li, P. Ni, D. Wang, K. Huang, J. Huang, and X. Tang, "A filter-less scheme for frequency 16-tupling millimeter-wave generation based on double parallel DPMZM," Laser J. **42**, 32–36 (2021).
20. X.-B. Wang, J. Yang, Y.-Y. Gao, and Y.-Y. Kang, "Frequency 16-tupling ROF system based on cascaded Mach-Zehnder modulators," J. Optoelectron. Laser **31**, 1262–1269 (2020).
21. R. Arya and J. Zacharias, "Performance improved tunable millimeter-wave signal generation employing UFBG based AOTF with bit walk-off effect compensation," Microw. Opt. Technol. Lett. **61**, 1221–1230 (2018).
22. P. Guo, Z. Lai, Z. Zhang, X. Fang, and Y. Shang, "Scheme to eliminate the time shift of code edges based on the optimal transmission point of a DP-MZM," Appl. Opt. **62**, 5652–5659 (2023).
23. Z.-H. Zhu, S.-H. Zhao, Z.-S. Yao, Q.-G. Tan, Y.-J. Li, X.-C. Chu, W. Xiang, and G.-H. Zhao, "A modified scheme for generation of optical millimeter-wave signal with carrier suppression modulation," J. Optoelectron. Laser **23**, 681–686 (2012).
24. C. Kavitha and C. T. Manimegalai, "A bidirectional RoF system for the multi-band signal with mitigation of the nonlinear effects," IETE J. Res. **69**, 7621–7633 (2024).
25. X. Chen, Z. Li, W. Ba, S. Dai, X. Chen, J. Liang, and H. Xiao, "A novel method to generate and transmit 40-tupling frequency millimeter wave over fiber based on remodulation of MZMs," Heliyon **9**, e14221 (2023).